

See discussions, stats, and author profiles for this publication at: <https://www.researchgate.net/publication/261439426>

Top-Seeded Solution Crystal Growth and Functional Properties of Polar LiFeP₂O₇

ARTICLE *in* CRYSTAL GROWTH & DESIGN · APRIL 2012

Impact Factor: 4.89 · DOI: 10.1021/cg3001587

CITATIONS

12

READS

39

2 AUTHORS:



Weiguo Zhang

University of Houston

26 PUBLICATIONS 356 CITATIONS

[SEE PROFILE](#)



Shiv Halasyamani

University of Houston

267 PUBLICATIONS 5,781 CITATIONS

[SEE PROFILE](#)

Top-Seeded Solution Crystal Growth and Functional Properties of Polar LiFeP_2O_7

Weiguo Zhang and P. Shiv Halasyamani*

Department of Chemistry, University of Houston, 136 Fleming Building, Houston, Texas 77204, United States

S Supporting Information

ABSTRACT: Large single crystals of LiFeP_2O_7 , a multifunctional polar material, were successfully grown by using a top-seeded solution growth (tssg) technique. The morphologies of the single crystals with different rotation speeds are described. Functional properties such as second-harmonic generation (SHG), piezoelectricity, pyroelectricity, and ferroelectricity were measured. LiFeP_2O_7 is SHG active, with an SHG efficiency of approximately $200 \times \alpha_{\text{SiO}_2}$ using 1064 nm radiation. The material is piezoelectric, with a d_{33} value of 1.2 pC/N, and pyroelectric, with pyroelectric coefficients of $9.25 \mu\text{C}/\text{m}^2\text{K}$ (1 kHz) and $10.6 \mu\text{C}/\text{m}^2\text{K}$ (50 Hz) at 60 °C. Although polar, LiFeP_2O_7 is not ferroelectric; that is, the polarization is not “switchable”. Optical spectra indicate that the absorption edge is approximately 480 nm, with transmission up to 4.3 μm .



INTRODUCTION

Multifunctional materials, especially multiferroics, have attracted much attention attributable to their potential of mutual polarization and magnetization control.^{1–13} The synthesis of multiferroic materials is an ongoing challenge as ferroelectricity and magnetic ordering are often mutually exclusive.¹⁴ For ferroelectric behavior, the material in question must crystallize in one of 10 polar crystal classes (1, 2, 3, 4, 6, m, mm2, 3m, 4mm, or 6mm).¹⁵ In addition, the macroscopic polarization must be reversible, or “switchable”, in the presence of an external electric field.¹⁶ With regards to magnetic ordering, ferro-, antiferro-, and ferrimagnetism are possible, depending on the interaction between the unpaired electron(s). Materials that exhibit both ferroelectricity and magnetic ordering are rare.^{17–30} A polar material that does exhibit magnetic ordering is LiFeP_2O_7 . LiFeP_2O_7 was first synthesized by Genkina et al.³¹ in 1985. The material is polar, crystallizing in the monoclinic space group $P2_1$. In 1990, Riou et al.³² redetermined the structure and also investigated the magnetic behavior. They determined that LiFeP_2O_7 is antiferromagnetic with a T_N of approximately 20 K, which was confirmed later by neutron diffraction and symmetry analysis.³³ Analysis and explanation of the magnetic structure were done by Whangbo et al.³⁴ In addition to the magnetic behavior, ionic conductivity of the Li^+ was investigated as potential applications for lithium rechargeable batteries.^{35,36} Most recently, the crystal structure, magnetic measurements, and infrared spectra of LiFeP_2O_7 solid solutions with Cr^{3+} were investigated.³⁷ To the best of our knowledge, no additional functional properties were investigated, even though the material is polar.

In this Article, we report on the single crystal growth of LiFeP_2O_7 using a top seeded solution growth technique. In addition to investigating the morphologies of the crystal, we

measured functional properties (second-harmonic generation, piezoelectricity, and polarization).

EXPERIMENTAL SECTION

Polycrystalline LiFeP_2O_7 Synthesis. Polycrystalline LiFeP_2O_7 was synthesized by solid-state methods. Stoichiometric amounts of LiH_2PO_4 (Alfa Aesar, 97%), Fe_2O_3 (Fisher Scientific, Certified), and $\text{NH}_4\text{H}_2\text{PO}_4$ (Alfa Aesar, 98.0%) were ground thoroughly, packed tightly in a platinum crucible, and heated to 200 °C for 10 h to decompose ammonium dihydrogen phosphate, and then 600 °C for 20 h and 850 °C for 20 h with intermittent regrindings. The purity of polycrystalline LiFeP_2O_7 was confirmed by powder XRD (see Figure S1).

Single Crystal Growth of LiFeP_2O_7 . Single crystals of LiFeP_2O_7 were grown by the top seeded solution growth (tssg) method. Polycrystalline LiFeP_2O_7 was mixed thoroughly with LiH_2PO_4 and $\text{NH}_4\text{H}_2\text{PO}_4$ with the molar ratio $\text{LiFeP}_2\text{O}_7:\text{LiH}_2\text{PO}_4:\text{NH}_4\text{H}_2\text{PO}_4 = 1:0.2:0.2$. The mixture was heated to 1100 °C in a platinum crucible in a vertical furnace equipped with a Pt–Rh/Pt thermocouple and a Al-808P controller. The temperature was held for 20 h to form a homogeneous melt. Once a homogeneous melt had formed, a piece of platinum wire held on an alumina rod was dipped into melt. The melt was then cooled at a rate 5 °C/h. At 1030 °C, small crystals spontaneously nucleated on the platinum wire. These small crystals were carefully extracted and confirmed to be single phase by powder XRD (see Figure 1). The exact saturation temperature then was determined by observing the growth or dissolution of crystal seed when soaking in the melt. After several growth runs with a seed crystal, a crystal of sufficient size was obtained to cut as an oriented crystal seed (see Figure S2). To obtain a large and high-quality single crystal, an oriented seed was introduced into homogeneous melt with a rotating rate of 7–12 rpm at 2 °C higher than the saturation temperature, followed by decreasing the temperature to the saturation

Received: February 2, 2012

Revised: March 5, 2012

Published: March 7, 2012

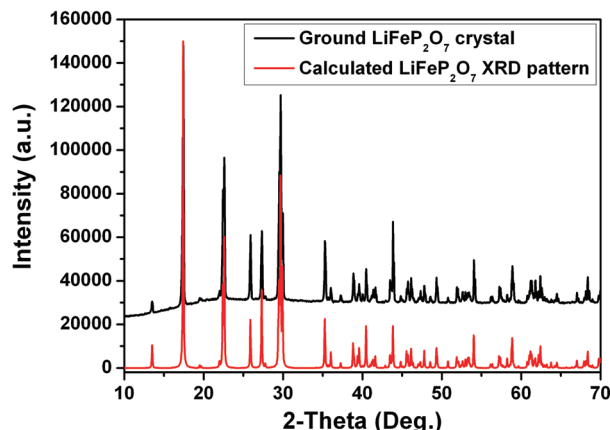


Figure 1. Calculated and observed powder XRD patterns for single crystal LiFeP_2O_7 .

point in 30 min. From the saturation temperature, the melt was cooled at a rate of $0.2\text{ }^\circ\text{C}$ per day to about $1\text{ }^\circ\text{C}$ below the saturation point. After 5 days growth, an as-grown single crystal was then hung above the melt surface and cooled slowly to room temperature. As-grown single crystals along $[010]$ orientation were obtained using the same procedure under different rotation speeds (see Figure 2).

Powder Diffraction. Powder X-ray diffraction (XRD) measurements on polycrystalline and ground single crystal LiFeP_2O_7 were carried out with a PANalytical X'Pert PRO diffractometer equipped with $\text{Cu K}\alpha$ radiation ($\lambda = 1.54056\text{ \AA}$) in the 2θ range from 10° to 70° . Some of the natural faces of the single crystal were indexed by XRD. The other small faces that cannot be checked by XRD were confirmed by measuring the angles relative to the known faces. The XRD patterns and measured angles are deposited in the Supporting Information (see Figures S3–S6 and Table S1).

TG/DTA Analysis. Thermogravimetric and differential thermal analyses (TG/DTA) of LiFeP_2O_7 were performed on an EXSTAR

TG/DTA 6300 thermal analysis system (SII Nano Technology Inc.). 13.0 mg of pure and polycrystalline LiFeP_2O_7 was placed in a platinum pan and heated/cooled at the rate of $10\text{ }^\circ\text{C}/\text{min}$ in the temperature range between 20 and $1100\text{ }^\circ\text{C}$ under N_2 atmosphere. After the TG/DTA measurement, the residue in the platinum pan was checked again by powder XRD (see Figure S7).

Optical Spectra Measurement. UV-visible reflectance data were collected on a Perkin-Elmer LAMBDA 1050 scan UV-vis-NIR spectrophotometer over the 200 – 2000 nm spectral range at room temperature. A piece of single crystal was ground into fine powder, and poly tetrafluoroethylene was used as a reference material. The reflectance spectrum was converted to absorbance using the Kubelka-Munk function.^{38,39} Infrared transmission spectra were recorded on a Matteson FTIR 5000 spectrometer in the 400 – 4000 cm^{-1} range perpendicular to the (020) plane.

Second Harmonic Generation (SHG). Powder SHG measurements were performed on a modified Kurtz-NLO system⁴⁰ using a pulse Nd:YAG laser with a wavelength of 1064 nm . A detailed description of the equipment and methodology has been published elsewhere.⁴¹ As the powder SHG efficiency has been shown to depend strongly on particle size,⁴⁰ the reported materials were ground and sieved into distinct particle size ranges (<20 , 20 – 45 , 45 – 63 , 63 – 75 , 75 – 90 , $>90\text{ }\mu\text{m}$). Relevant comparisons with known SHG materials were made by grinding and sieving crystalline $\alpha\text{-SiO}_2$ into the same particle size ranges. No index matching fluid was used in any of the experiments.

Piezoelectric Measurements. Direct piezoelectric coefficients were collected on a YE2730A d_{33} meter (APC international, Ltd.). According to the IEEE standard,⁴² a Y-cut sample (faces perpendicular to b -axis) was cut from LiFeP_2O_7 single crystal with the size of 5.0 mm (width) $\times 8.0\text{ mm}$ (length) $\times 0.5\text{ mm}$ (thickness). In addition, converse piezoelectric measurements were performed using a Radian Technologies RT66A piezoelectric test system with a TREK (model 609E-6) high-voltage amplifier, Precision Materials Analyzer, Precision High-Voltage Interface, and MTI 2000 Fotonic Sensor. For converse piezoelectric measurements, the sample was covered by silver paste on

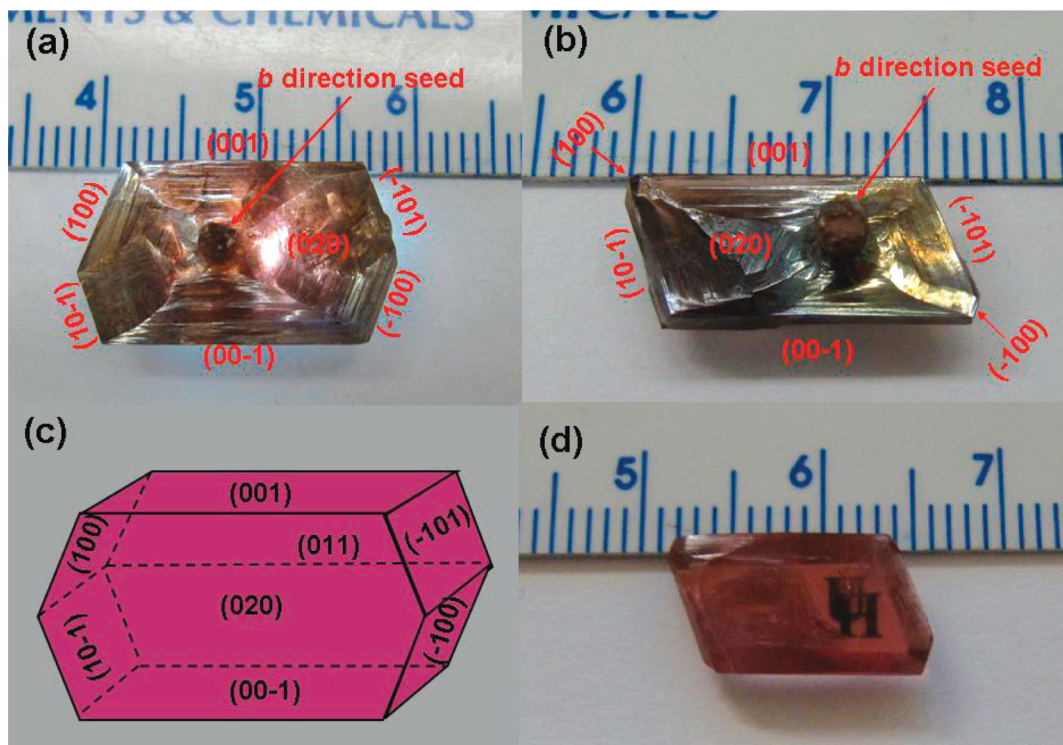


Figure 2. As-grown crystals at rotation speeds (a) 7 rpm and (b) 12 rpm, (c) simulated morphology, and (d) polished faces parallel to (010) plane. Note that the good transparency in (d) indicates high crystal quality.

both sides as electrodes and cured at 400 °C for 3 h. The applied voltage for the Y-cut sample was set to 900 V.

Polarization Measurements. The Y-cut crystal used in the piezoelectric measurements was also used in the polarization measurements. The polarization was measured on a Radian Technologies RT66A Ferroelectric Test System with a TREK high voltage amplifier between 20 and 120 °C in 20 °C increments in a Delta 9023 environmental test chamber. The temperature was allowed to stabilize before the polarization was measured. The unclamped pyroelectric coefficient, defined as dP/dT (change in the polarization with respect to the change in temperature), was determined by measuring the polarization as a function of temperature. A detailed description of the methodology has been published elsewhere.⁴¹ To determine the ferroelectric behavior, the polarization loop was measured at room temperature under a static electric field of 4–24 kV/cm from 50 to 1000 Hz.

RESULTS AND DISCUSSION

Synthesis and Characterization of Polycrystalline LiFeP₂O₇. Polycrystalline LiFeP₂O₇ was synthesized by solid-state reaction techniques. Stoichiometry and homogeneity of the starting mixture are both important for synthesizing a pure polycrystalline and single phase LiFeP₂O₇. Powder XRD patterns of the polycrystalline phase are in good agreement with the calculated pattern derived from the single crystal data.³² Figure S1 shows the experimental and calculated patterns of powder XRD of polycrystalline LiFeP₂O₇. As there is no report of thermal properties of LiFeP₂O₇, TG/DTA measurements were performed under 1100 °C to determine if there is melting or a phase transition. As seen in Figure 3, there

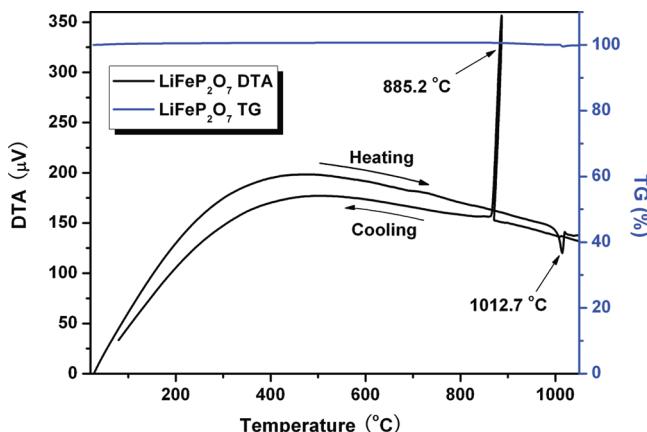


Figure 3. TG/DTA measurements of polycrystalline LiFeP₂O₇.

is an endothermic peak around 1013 °C during heating, and a very sharp exothermic peak around 885 °C during cooling. There is no weight loss during the whole process, which suggests homogeneous melting. The powder XRD pattern of the residue in the platinum pan indicates the main phase of LiFeP₂O₇ is mixed with another unknown phase (see Figure S7). This likely indicates that LiFeP₂O₇ partially decomposes upon melting.

Growth and Morphologies of LiFeP₂O₇ Crystal. At the same molar ratios of starting materials (LiFeP₂O₇:LiH₂PO₄:NH₄H₂PO₄ = 1:0.2:0.2), growth conditions at different rotation speeds were carried out. Well-faceted pink single crystals of LiFeP₂O₇ were grown by the tssg method along the [010] direction. Figure 2 shows the as-grown crystals with indexed (*hkl*) planes. As shown in Figure 2, all of the crystals present (100), (001), (101), (100), (001), and (101)

planes parallel to the *b*-axis. The differences between the crystals grown at different rotation speed are evident from the sizes of the planes. Clearly, the size of the (100) plane is much larger at lower rotation speed (7 rpm) than at higher rotation speed (12 rpm). At higher rotation speeds, the (100) plane almost disappears. Although the growth mechanism is not well understood, diffusion-controlled crystal growth can aid in our understanding.⁴³ The diffusion layer between the crystal and melt controls the transport speed of the “growth unit” between the crystal and the melt. The “growth unit” is defined as the “unit” from the flux that adheres to the crystal surface and promotes crystal growth. A thicker diffusion layer results in a slower transport speed of the “growth unit”. The thickness of this diffusion layer is related to the rotation speed. Lower rotation speeds result in a thicker diffusion layer. Thus, at lower rotation speeds, the growth rate of the crystal is determined by the thickness of the diffusion layer regardless of the growth rate along specific crystallographic directions. Conversely, at higher rotation speeds, the growth around crystal faces is faster attributable to the thinner diffusion layer. In this situation, a faster growth rate along certain directions is dominant. As discussed elsewhere,³² there is a [FeP₂O₇][−] tunnel along the *a*-axis. It is suggested that crystal growth is much easier going into the tunnel than packing on the chain.⁴⁴ This also suggests that the growth rate along the *a*-axis is much higher than in other directions. This is possibly the reason for the disappearance of the (100) plane, as the plane shrinks quickly along the higher growth rate directions.

Optical Spectra Analyses of LiFeP₂O₇ Crystal. The UV-vis diffuse reflectance spectra, as shown in Figure 4,

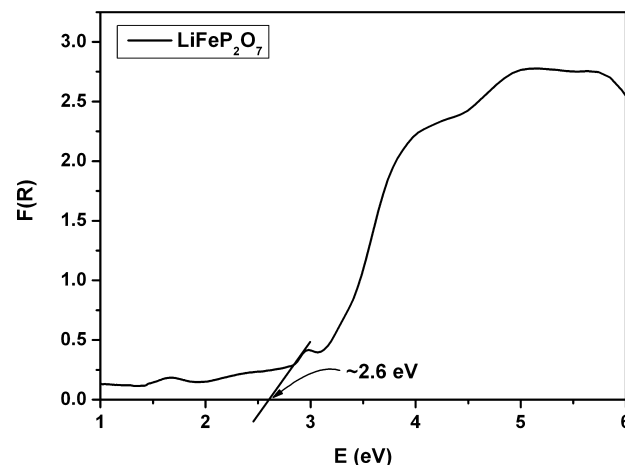


Figure 4. UV-vis diffuse reflectance spectroscopy data for ground single crystal LiFeP₂O₇.

indicate the absorption energy for LiFeP₂O₇ is approximately 2.6 eV. Absorption (K/S) data were calculated from the Kubelka–Munk function.³⁹

$$F(R) = \frac{(1 - R)^2}{2R} = \frac{K}{S}$$

where *R* represents the reflectance, *K* is the absorption coefficient, and *S* is the scattering factor. In a K/S versus *E* (eV) plot, extrapolating the linear part of the rising curve to zero provides the onset of absorption at 2.6 eV (see Figure 4). There are some broad bands in the range of 3–6 eV attributable to the d–d transitions of Fe and Fe to ligand

charge transfer.⁴⁵ The onset of bands indicates the UV absorption edge of LiFeP₂O₇ single crystal is around 480 nm. In Figure 5, the infrared transmission spectra of (010) wafer

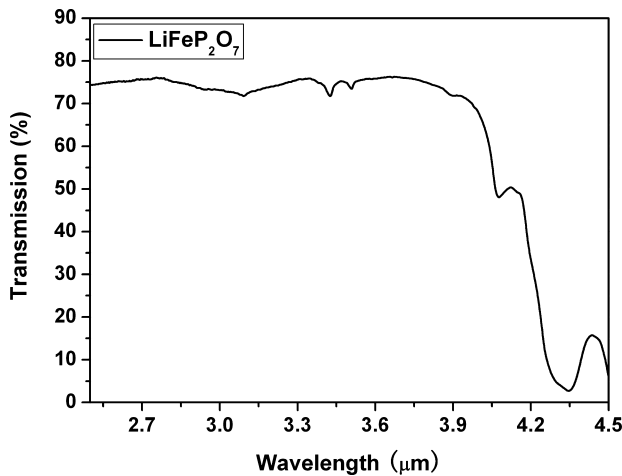


Figure 5. Mid-IR transmission spectra of the LiFeP₂O₇ crystal perpendicular to the (010) plane.

suggest that LiFeP₂O₇ single crystal can transmit up to 4.3 μm. Taking into consideration UV-vis diffuse reflectance spectra and infrared transmission spectra, LiFeP₂O₇ single crystal exhibits a very broad transmission range (0.48–4.3 μm) as compared to widely used commercial crystals such as β -BaB₂O₄ (BBO) (0.189–3.5 μm),⁴⁶ LiB₃O₅ (LBO) (0.16–2.6 μm),⁴⁷ and KH₂PO₄ (KDP) (0.176–1.4 μm).⁴⁸ This indicates single crystal LiFeP₂O₇ is a new promising candidate for nonlinear optical applications.

Second-Harmonic Generation. Because LiFeP₂O₇ crystallizes in the noncentrosymmetric and polar space group, P2₁, SHG measurements were performed. Powder SHG measurements using 1064 nm radiation revealed efficiencies of approximately 200 × α -SiO₂ for LiFeP₂O₇ in the 45–63 μm particle size range. Additional SHG measurements, Figure 6, SHG efficiency versus particle size (20–125 μm), revealed that LiFeP₂O₇ is type-1 phase-matchable and falls into the class A category of SHG materials.⁴⁰

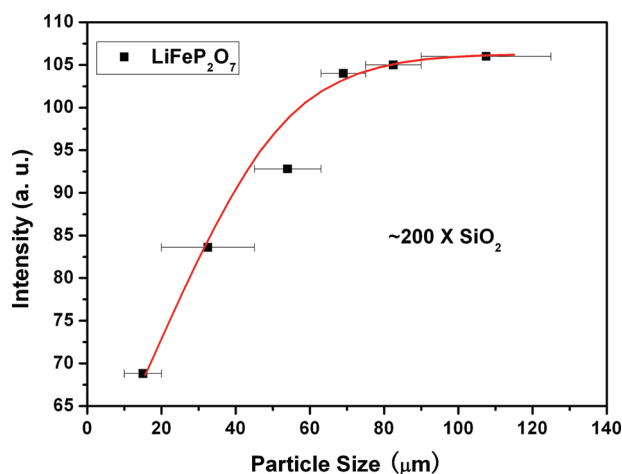


Figure 6. Phase matching, that is, particle size versus SHG intensity, data for LiFeP₂O₇. The curve is drawn to guide the eye and is not a fit to the data.

Piezoelectricity of LiFeP₂O₇ Crystal. Piezoelectric measurements were performed on a Y-cut crystal by direct and converse methods. The estimated d_{22} values are listed in Table 1 along with comparisons to SiO₂ and LiTaO₃.⁴⁹ The

Table 1. Piezoelectric Coefficients from Direct and Converse Methods

| piezoelectric coefficients | LiFeP ₂ O ₇ | | SiO ₂ ^a (pm/V) | LiTaO ₃ ^a (pm/V) |
|----------------------------|-----------------------------------|-------------|---|---|
| | dir. (pC/N) | con. (pm/V) | | |
| d_{11} | 0 | 0 | -2.31 | 0 |
| d_{22} | 1.2 | 1.9 | 0 | 7 |
| d_{33} | 0 | 0 | 0 | 8 |

^aFrom ref 49.

piezoelectric data from the converse method have been deposited in the Supporting Information (see Figure S8). The d value derived from converse method matches well with the direct method.

Pyroelectricity and Ferroelectricity of LiFeP₂O₇ Crystal. The unclamped pyroelectric coefficient was determined by measuring the polarization as a function of temperature under 800 V at different frequencies in the temperature range 20–120 °C. The polarization versus temperature data, and the temperature and frequency dependence of the pyroelectric coefficient, have been deposited in the Supporting Information (see Figures S9 and S10, respectively). The pyroelectric coefficient ranges between 9.25 μ C/m²K (1kHz) and 10.5 μ C/m²K (50 Hz) at 60 °C. As the material is polar, ferroelectric measurements were performed to investigate any polarization reversibility. Figure 7 shows the polarization versus electric field at various frequencies and voltages. Clearly, a linear relationship between polarization and electric field is observed, indicating that LiFeP₂O₇ is not ferroelectric. In other words, the polarization cannot be switched under an external electric field. To understand this irreversibility, the local polarizations in the materials need to be examined. The polarity in LiFeP₂O₇ is attributable to the local dipole moments observed in the FeO₆ octahedra and PO₄ tetrahedra. For the materials to exhibit ferroelectric behavior, the polarization must be “switchable”, or “reversible” in the presence of an external electric field. For d⁰ transition metals in octahedral oxide coordination environments, it is possible for the cation to be “switched” from one corner, edge, or face to the opposite, for example, BaTiO₃ (corner) and LiNbO₃ (face),^{50,51} in the presence of an external electric field resulting in ferroelectric behavior. In LiFeP₂O₇, infinite [FeP₂O₁₁]_∞ chains are observed that share corners, in two-dimensions, to create the three-dimensional framework. The reversal in the macroscopic polarization would require substantial rearrangements of the polyhedra, as well as metal–oxygen bond breaking. Thus, it is suggested that polarization reversal is highly energetically unfavorable, and therefore LiFeP₂O₇ is not ferroelectric.

CONCLUSIONS

We have successfully grown large crystals of polar LiFeP₂O₇ by the top-seeded solution growth method. In addition, we have demonstrated that different rotation speeds will influence the morphologies of the as-grown crystals. Although LiFeP₂O₇ is polar, the polarization is not reversible, indicating the material is not ferroelectric. Optical data of the LiFeP₂O₇ crystal reveal a broad transmission region up to 4.3 μm suggesting the material

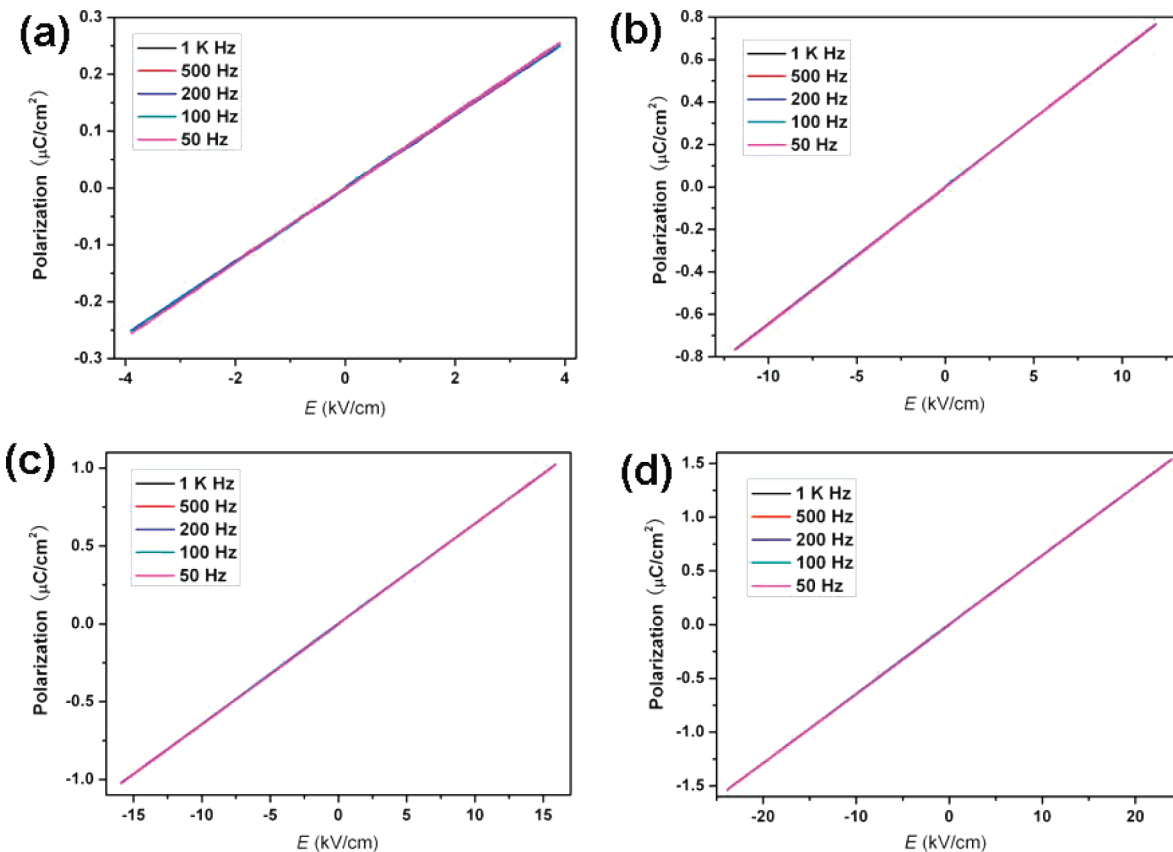


Figure 7. Polarization versus electric field plots at (a) 4 kV/cm, (b) 12 kV/cm, (c) 16 kV/cm, and (d) 24 kV/cm at different frequencies for a Y-cut LiFeP_2O_7 single crystal. Note that there is no hysteresis, indicating the material is not ferroelectric; that is, the polarization is not reversible.

has nonlinear optical applications. Magneto-electric measurements below 20 K are currently underway to investigate any multiferroic behavior.

■ ASSOCIATED CONTENT

S Supporting Information

Figures S1–S10 and Table S1. This material is available free of charge via the Internet at <http://pubs.acs.org>.

■ AUTHOR INFORMATION

Corresponding Author

*E-mail: psh@uh.edu.

Notes

The authors declare no competing financial interest.

■ ACKNOWLEDGMENTS

We thank the Robert A. Welch Foundation (Grant E-1457) and the Texas Center for Superconductivity for support. We also thank Martin Donakowski (Northwestern University) for performing the diffuse reflectance measurements. Diffuse-reflectance spectra were obtained at the Keck Biophysics Facility at Northwestern University that is supported by grants from the W.M. Keck Foundation, Northwestern University, the NIH, the Rice Foundation, and the Robert H. Lurie Comprehensive Cancer Center.

■ REFERENCES

- Wang, L.; Wang, D.; Cao, Q.; Zheng, Y.; Xuan, H.; Gao, J.; Du, Y. *Sci. Rep.* **2012**, *2*, 1.
- Wu, S. M.; Cybart, S. A.; Yu, P.; Rossell, M. D.; Zhang, J. X.; Ramesh, R.; Dynes, R. C. *Nat. Mater.* **2010**, *9*, 756.
- Mostovoy, M. *Nat. Mater.* **2010**, *9*, 188.
- Tokunaga, Y.; Furukawa, N.; Sakai, H.; Taguchi, Y.; Arima, T.-H.; Tokura, Y. *Nat. Mater.* **2009**, *8*, 558.
- Ramesh, R. *Nature* **2009**, *461*, 1218.
- Ramesh, R.; Spaldin, N. A. *Nat. Mater.* **2007**, *6*, 21.
- Tokura, Y. *Science* **2006**, *312*, 1481.
- Eerenstein, W.; Mathur, N. D.; Scott, J. F. *Nature* **2006**, *442*, 759.
- Khomskii, D. I. *J. Magn. Magn. Mater.* **2006**, *306*, 1.
- Spaldin, N. A.; Fiebig, M. *Science* **2005**, *309*, 391.
- Hur, N.; Park, S.; Sharma, P. A.; Ahn, J. S.; Guha, S.; Cheong, S.-W. *Nature* **2004**, *429*, 392.
- Kimura, T.; Goto, T.; Shintani, H.; Ishizaka, K.; Arima, T.; Tokura, Y. *Nature* **2003**, *426*, 55.
- Fiebig, M.; Lottermoser, T.; Frohlich, D.; Goltsev, A. V.; Pisarev, R. V. *Nature* **2002**, *419*, 818.
- Hill, N. A. *J. Phys. Chem. B* **2000**, *104*, 6694.
- Hahn, T. *International Tables for Crystallography*; Kluwer Academic: Dordrecht, The Netherlands, 2006; Vol. A: Space Group Symmetry.
- Lines, M. E.; Glass, A. M. *Principles and Applications of Ferroelectrics and Related Materials*; Oxford University Press: Oxford, 1991.
- Ito, T.; Ushiyama, T.; Yanagisawa, Y.; Kumai, R.; Tomioka, Y. *Cryst. Growth Des.* **2011**, *11*, 5139.
- Povillain, P.; Sousa, R.; Gallais, Y.; Sacuto, A.; Measson, M. A.; Colson, D.; Forget, A.; Bibes, M.; Barthelemy, A.; Cazayous, M. *Nat. Mater.* **2010**, *9*, 975.
- Kim, S. W.; Chang, H. Y.; Halasyamani, P. S. *J. Am. Chem. Soc.* **2010**, *132*, 17684.
- Claridge, J. B.; Hughes, H.; Bridge, C. A.; Allix, M.; Suchomel, M. R.; Niu, H.; Kuang, X.; Rosseinsky, M. J.; Bellido, N.; Grebille, D.

- Perez, O.; Simon, C.; Pelloquin, D.; Blundell, S. J.; Lancaster, T.; Baker, P. J.; Pratt, F. L.; Halasyamani, P. S. *J. Am. Chem. Soc.* **2009**, *131*, 14000.
- (21) Mao, X.; Wang, W.; Chen, X.; Lu, Y. *Appl. Phys. Lett.* **2009**, *95*, 082901.
- (22) Ye, F.; Ren, Y.; Fernandez-Bace, J. A.; Mook, H. A.; Lynn, J. W.; Chaudhury, R. P.; Wang, Y.-Q.; Lorenz, B.; Chu, C. W. *Phys. Rev. B* **2008**, *78*, 193101.
- (23) Vajk, O. P.; Kenzelmann, M.; Lynn, J. W.; Kim, S. B.; Cheong, S.-W. *J. Appl. Phys.* **2006**, *99*, 08E301.
- (24) Cruz, C. R.; Yen, F.; Lorenz, B.; Gospodinov, M. M.; Chu, C. W.; Ratcliff, W.; Lynn, J. W.; Park, S.; Cheong, S.-W. *Phys. Rev. B* **2006**, *73*, 100406.
- (25) Kenzelmann, M.; Harris, A. B.; Jonas, S.; Broholm, C.; Schefer, J.; Kim, S. B.; Zhang, C. L.; Cheong, S.-W.; Vajk, O. P.; Lynn, J. W. *Phys. Rev. Lett.* **2005**, *95*, 087206.
- (26) Azuma, M.; Takata, K.; Saito, T.; Ishiwata, S.; Shimakawa, Y.; Takano, M. *J. Am. Chem. Soc.* **2005**, *127*, 8889.
- (27) Zheng, H.; Wang, J.; Loftland, S. E.; Ma, Z.; Mohaddes-Ardabili, L.; Zhao, T.; Salamanca-Riba, L.; Shinde, S. R.; Ogale, S. B.; Bai, F.; Viehland, D.; Jia, Y.; Schlom, D. G.; Wuttig, M.; Roytburd, A.; Ramesh, R. *Science* **2004**, *303*, 661.
- (28) Sharan, A.; Lettieri, J.; Jia, Y.; Tian, W.; Pan, X.; Schlom, D. G.; Gopalan, V. *Phys. Rev. B* **2004**, *69*, 214109.
- (29) Ederer, C.; Spaldin, N. A. *Phys. Rev. B* **2006**, *74*, 020201.
- (30) Scott, J. F. *Rep. Prog. Phys.* **1979**, *42*, 1055.
- (31) Genkina, E.; Maximov, B.; Timofeeva, V.; Bykov, A.; Melnikov, O. *Dokl. Akad. Nauk SSSR* **1985**, *284*, 864.
- (32) Riou, D.; Nguyen, N.; Benloucif, R.; Raveau, B. *Mater. Res. Bull.* **1990**, *25*, 1363.
- (33) Rousse, G.; Rodriguez-Carvajal, J.; Wurm, C.; Masquelier, C. *Solid State Sci.* **2002**, *4*, 973.
- (34) Whangbo, M.-H.; Dai, D.; Koo, H.-J. *Dalton Trans.* **2004**, *19*, 3019.
- (35) Vitins, G.; Kanepe, Z.; Vitins, A.; Ronis, J.; Dindune, A.; Lusis, A. J. *Solid State Electrochem.* **2000**, *4*, 146.
- (36) Wurm, C.; Morcrette, M.; Rousse, G.; Dupont, L.; Masquelier, C. *Chem. Mater.* **2002**, *14*, 2701.
- (37) Bih, H.; Saadoune, I.; Ehrenber, H.; Fuess, H. *J. Solid State Chem.* **2009**, *182*, 821.
- (38) Tauc, J. *Mater. Res. Bull.* **1970**, *5*, 721.
- (39) Kubelka, P.; Munk, F. Z. *Tech. Phys.* **1931**, *12*, 593.
- (40) Kurtz, S. K.; Perry, T. T. *J. Appl. Phys.* **1968**, *39*, 3798.
- (41) Ok, K. M.; Chi, E. O.; Halasyamani, P. S. *Chem. Soc. Rev.* **2006**, *35*, 710.
- (42) *IEEE Standard on Piezoelectricity*; IEEE Inc.: New York, 1988.
- (43) Mersmann, A. *Crystallization Technology Handbook*; Marcel Dekker, Inc.: New York, 2001.
- (44) Xu, D. In *Science and Technology of Crystal Growth*; Zhang, K. C., Zhang, L. H., Eds.; Science: Beijing, 1997 (in Chinese).
- (45) Miessler, G. L.; Tarr, D. A. *Inorganic Chemistry*, 3rd ed.; Pearson Education, Inc.: New Jersey, 2004.
- (46) Klein, R. S.; Kugel, G. E.; Maillard, A.; Sifi, A.; Polgar, K. *Opt. Mater.* **2003**, *22*, 163.
- (47) Chen, C.; Wu, Y.; Jiang, A.; Wu, B.; You, G.; Li, R.; Lin, S. J. *Opt. Soc. Am. B* **1989**, *6*, 616.
- (48) Sliker, T. R.; Burlage, S. R. *J. Appl. Phys.* **1963**, *34*, 1837.
- (49) Gao, Z.; Tao, X.; Yin, X.; Zhang, W.; Jiang, M. *Appl. Phys. Lett.* **2008**, *93*, 252906.
- (50) Shirane, G.; Danner, H.; Pepinsky, R. *Phys. Rev.* **1957**, *105*, 846.
- (51) Abrahams, S. C.; Hamilton, W. C.; Reddy, J. M. *J. Phys. Chem. Solids* **1966**, *27*, 1013.